

Effect of Electromechanical Coupling on Static Deformations and Natural Frequencies

Jiang Jin and Romesh C. Batra

Abstract—A two-way coupled electromechanical theory is used to study static deformations and free vibrations of a laminated hybrid rectangular plate comprised of either piezoceramic (PZT) layers or patches embedded at arbitrary locations in graphite/epoxy layers. A first-order shear deformation theory is used to develop equations for the plate which are solved by the finite-element method (FEM) using eight-node isoparametric elements. Static deflections and natural frequencies computed with open-circuited PZT layers are found to differ significantly from those of grounded PZT layers.

I. INTRODUCTION

MICROELECTROMECHANICAL SYSTEMS (MEMS), consisting of multilayered diaphragms of piezoelectric (PZT)¹ and nonpiezoelectric materials, often are used as sensors and actuators. They function by converting either electrical energy into mechanical energy or vice versa. The PZT actuators usually are poled in the thickness direction. The application of an electric field in the thickness direction causes the actuator's lateral dimensions to change and induce a strain in the host structure. In order to effectively design MEMS and smart structures, one needs simple models that consider electromechanical deformations of PZTs and account for the interaction between MEMS and the host structure.

Modeling techniques involve either one-way or two-way coupling between the electric and the mechanical deformations. In the former theories, the actuation effect of a PZT actuator is replaced by equivalent forces on the host structure, and the electric displacement in a PZT layer is determined by the strain field. In the latter theories, the electric displacement and the mechanical response are coupled together in the sense that the electric field and the mechanical deformations of a PZT actuator determine forces it exerts on the host structure.

Crawley and Lazarus [1] and Crawley and de Luis [2] used the one-way coupled theory to analyze their experimental setup and correlate computed results with the test values. Wang and Rogers [3] and Yao *et al.* [4] used the classical laminated plate theory to analyze a laminated

plate with uniformly distributed PZT actuators. Shah *et al.* [5] used Mindlin's (or the first-order shear deformation theory (FSDT)) plate theory and a nine-node quadrilateral element to analyze the problem by the finite-element method (FEM). Other works using the FEM and the FSDT to study hybrid laminated structures include those of Ghosh and Batra [6], [7] and Batra and Ghosh [8] to control the shape and annul vibrations, Chandrashekhara and Bhatia [9] to control the buckling of a plate, Chandrashekhara and Tenneti [10] to suppress thermally induced vibrations, and Varadarajan *et al.* [11] to control the shape of a structure. Researchers using the second type of theories include Allik and Hughes [12] who developed a general FEM for studying vibrations of a hybrid body, and Batra and Liang [13] who developed a finite element (FE) code using eight-node isoparametric brick elements to analyze transient-finite, three-dimensional deformations of a hybrid body comprised of orthotropic nonpiezoelectric and PZT materials. Batra and Liang [13] accounted for both material and geometric nonlinearities. It was shown that the consideration of terms quadratic in the electric field in the constitutive relations improved the agreement between the computed transverse deflections of a PZT layer and those observed by Crawley and Lazarus [1]. The code was used by Batra and Geng [14] to delineate the enhancement in the dynamic buckling load of a column and a plate by activating PZT layers perfectly bonded to its surfaces. They [15] enhanced the code's capabilities to include viscoelastic material behavior and studied the damping induced by layers enclosed between the host structure and the PZT layers. Ha *et al.* [16] also included incompatible modes in their three-dimensional FE code, and Kim *et al.* [17] and Lim *et al.* [18] used a combination of 20-node brick, 13-node transition, and 9-node plate elements to describe the behavior of an isotropic plate instrumented with PZT sensors and actuators. Saravanos *et al.* [19] used a layerwise laminated plate theory, and Thornburgh and Chattopadhyay [20] used a higher-order laminated plate theory to study deformations of a smart structure.

Vidoli and Batra [21] used a mixed, three-dimensional variational principle [22] to derive two-dimensional equations for a piezoelectric plate. They used this theory to study cylindrical deformations of a transversely isotropic plate due to equal and opposite charges applied to its top and bottom surfaces. Batra and Vidoli [23] used the mixed variational principle [22] to deduce a K 'th-order two-dimensional linear theory for an anisotropic homogeneous PZT plate. They showed that it can capture boundary-layer effects near the clamped and the free edges. Also,

Manuscript received February 11, 2004; accepted October 29, 2004.

J. Jin is with the School of Civil Engineering, Nantong University, Nantong 226007, Jiangsu, People's Republic of China.

R. C. Batra is with the Department of Engineering Science and Mechanics, Virginia Polytechnic Institute and State University, Blacksburg, VA 24061 (e-mail: rbatra@vt.edu).

¹The abbreviation PZT is used to denote a generic rather than a specific piezoceramic material.

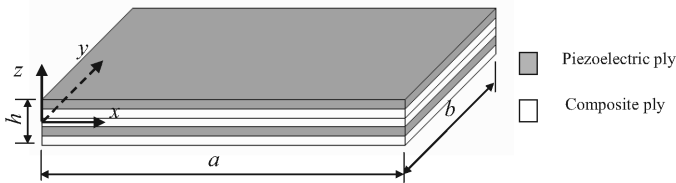


Fig. 1. A schematic of the problem studied.

through-the-thickness variation of the transverse shear and the transverse normal stresses agree well with those computed from the analytical solution of the three-dimensional piezoelectric equations. Vel and Batra [24], [25] have used the Eshelby-Stroh formalism to find analytical solutions for static deformations of a composite beam containing PZT patches. Vel *et al.* [26] have used a similar technique to analyze cylindrical bending vibrations of a piezoelectric composite plate. Yang *et al.* [27] and Batra *et al.* [28], [29] modeled PZT layers as membranes, but Vel *et al.* [26] accounted for their transverse deformations. Furthermore, Vel *et al.*'s [26] approach can accommodate PZT patches. We note that shear mode actuators have been studied by Vidoli and Batra [30] and Vel and Batra [31], [32].

Analyses based on three-dimensional deformations give detailed information and accurate results; however, they can be quite expensive for designing a MEMS because the design process is intrinsically iterative. Thus, simple models that capture nearly all of the physics of the system and are easy to use can be very helpful to designers.

Here a two-way coupled FSDT and eight-node isoparametric quadrilateral elements are used to analyze static deformations and vibrations of a thin laminated hybrid plate with rectangular PZT patches embedded at arbitrary locations. The primary contribution of this work is to show that the electromechanical coupling strongly influences natural frequencies of a hybrid laminated plate. It is established by analyzing structures with the top and the bottom surfaces of PZT layers either grounded or open circuited. Results computed with the FSDT are found to match well with those obtained from the three-dimensional commercial code ANSYS (Ansys, Inc., Canonsburg, PA). Results computed for nine-layer and three-layer thin hybrid laminated plates also agree well with the test findings of different investigators [2], [33]. Results have been computed for a cantilever plate and a rectangular plate with two opposite edges either clamped or simply supported, or all edges free.

II. PROBLEM FORMULATION

A schematic of the problem studied and the location of rectangular Cartesian coordinate axes are shown in Fig. 1. We consider a laminated hybrid composite plate with plies made of either a PZT material or a fiber-reinforced composite; each layer may be made of an orthotropic material. The PZT layers need not be symmetrically located about the midsurface of the plate. Furthermore, they need

not extend along the entire length and width of the plate. Said differently, segmented rectangular PZT patches may be bonded to the top and the bottom surfaces of the plate. Two adjacent plies are assumed to be perfectly bonded together with an adhesive layer of negligible thickness. The three-dimensional constitutive relation for an anisotropic piezoelectric layer can be written as:

$$\{\sigma\} = [c]\{\varepsilon\} - [e]\{E\}, \quad (1a)$$

$$\{D\} = [e]^T\{\varepsilon\} + [\xi]\{E\}, \quad (1b)$$

where $\{\sigma\} = (\sigma_{xx}, \sigma_{yy}, \sigma_{zz}, \sigma_{xy}, \sigma_{yz}, \sigma_{zx})^T$ and $\{\varepsilon\} = (\varepsilon_{xx}, \varepsilon_{yy}, \varepsilon_{zz}, 2\varepsilon_{xy}, 2\varepsilon_{yz}, 2\varepsilon_{zx})^T$ are, respectively, six-dimensional vectors of stresses and strains for infinitesimal deformations, $[c]$ is the 6×6 matrix of elastic constants, $[e]$ is the 6×3 matrix of piezoelectric constants, $[\xi]$ is the 3×3 matrix of electric permittivities, and $\{E\} = (E_x, E_y, E_z)^T$ and $\{D\} = (D_x, D_y, D_z)^T$ are three-dimensional vectors of the electric field and the electric displacement, respectively. The electric field is related to the electric potential ϕ by:

$$\{E\} = - \left(\frac{\partial \phi}{\partial x}, \frac{\partial \phi}{\partial y}, \frac{\partial \phi}{\partial z} \right)^T. \quad (2)$$

The PZT layer is poled in the z -direction and is assumed to be transversely isotropic about the z -axis. Thus, it has five nonzero piezoelectric constants: e_{31} , e_{32} , e_{33} , e_{15} , and e_{24} . For a nonpiezoelectric layer, $[e] = 0$.

The plate thickness is assumed to be small as compared to its in-plane dimensions. Because the transverse normal stress, σ_{zz} , is very small as compared to the in-plane stresses, we set $\sigma_{zz} = 0$ in (1a), solve it for ε_{zz} , and substitute the result in the remaining equations. We thus obtain:

$$\{\sigma\} = [\bar{c}]\{\varepsilon\} - [\bar{e}]\{E\}, \quad (3a)$$

$$\{D\} = [\bar{e}]^T\{\varepsilon\} + [\xi]\{E\}, \quad (3b)$$

where $[\bar{c}]$ and $[\bar{e}]$ are 5×5 and 5×3 matrices of the modified (or the reduced) elastic constants and piezoelectric coefficients, respectively. Note that $\{\sigma\}$ and $\{\varepsilon\}$ are now five-dimensional vectors. In most applications of plate-like structures, surface tractions and the electric potential are prescribed on the top and the bottom surfaces. Thus $|\sigma_{zz}| \ll \min(|\sigma_{xx}|, |\sigma_{yy}|)$, and $|E_z| \gg \max(|E_x|, |E_y|)$. A goal of this work is to analyze the influence of the electromechanical coupling upon the natural frequencies.

We use the following displacement field for the FSDT:

$$\begin{aligned} u(x, y, z, t) &= u_0(x, y, t) + z\psi_x(x, y, t), \\ v(x, y, z, t) &= v_0(x, y, t) + z\psi_y(x, y, t), \\ w(x, y, z, t) &= w_0(x, y, t), \end{aligned} \quad (4)$$

where u_0 , v_0 , and w_0 are displacements of a point on the midsurface of the plate, and ψ_x and ψ_y are rotations about the y - and the x -axes, respectively, of the normal to the midplane. Eq. (4) gives continuous displacements across

an interface between two adjoining layers, but generally result in discontinuous tractions across an interface. An alternative is to use a layerwise plate theory that significantly increases the number of unknowns. The electric field in the k th layer with $z_k \leq z \leq z_{k+1}$ in it is assumed to be given by:

$$\phi(x, y, z, t) = \phi_k(x, y, t) + \frac{z - z_k}{z_{k+1} - z_k} (\phi_{k+1}(x, y, t) - \phi_k(x, y, t)), \quad (5)$$

where ϕ_k and ϕ_{k+1} are the electric potentials on the bottom and the top surfaces of the k th layer, respectively. Thus, the electric field, E_z , in each layer does not vary with z .

Fields (4) and (5) give the following for the infinitesimal strains and the electric field at a point:

$$\{\varepsilon\} = \{\varepsilon_0\} + z\{\kappa\},$$

$$\{\varepsilon_0\} = \left(\frac{\partial u_0}{\partial x}, \frac{\partial v_0}{\partial y}, \frac{\partial u_0}{\partial y} + \frac{\partial v_0}{\partial x}, \frac{\partial w_0}{\partial x} + \psi_y, \frac{\partial w_0}{\partial y} + \psi_x \right)^T,$$

$$\{\kappa\} = (\kappa_x, \kappa_y, \kappa_{xy}, 0, 0)^T \quad (6)$$

$$= \left(\frac{\partial \psi_x}{\partial x}, \frac{\partial \psi_y}{\partial y}, \frac{\partial \psi_x}{\partial y} + \frac{\partial \psi_y}{\partial x}, 0, 0 \right)^T.$$

$$E_x^{(k)} = - \left(\frac{\partial \phi_k}{\partial x} + \frac{z - z_k}{z_{k+1} - z_k} \left(\frac{\partial \phi_{k+1}}{\partial x} - \frac{\partial \phi_k}{\partial x} \right) \right), \quad (7a)$$

$$E_y^{(k)} = - \left(\frac{\partial \phi_k}{\partial y} + \frac{z - z_k}{z_{k+1} - z_k} \left(\frac{\partial \phi_{k+1}}{\partial y} - \frac{\partial \phi_k}{\partial y} \right) \right), \quad (7b)$$

$$E_z^{(k)} = -(\phi_{k+1} - \phi_k)/(z_{k+1} - z_k). \quad (7c)$$

Here $\{E^{(k)}\}$ is the electric field in the k th layer.

Substitution from (6) and (7) into (3a) and integration of the resulting equation over the plate thickness give:

$$\{\bar{N}\} = [\bar{C}]\{\bar{\varepsilon}\} - [\bar{e}]\{\Delta\phi\}, \quad (8)$$

where:

$$\{\bar{N}\} = (N_{xx}, N_{yy}, N_{xy}, M_{xx}, M_{yy}, M_{xy}, Q_{yz}, Q_{xz})^T, \quad (9)$$

$$\{\bar{\varepsilon}\} = (\varepsilon_{0xx}, \varepsilon_{0yy}, 2\varepsilon_{0xy}, \kappa_x, \kappa_y, \kappa_{xy}, 2\varepsilon_{0yz}, 2\varepsilon_{0xz})^T, \quad (10)$$

$$(N_{xx}, N_{yy}, N_{xy}, Q_{yz}, Q_{xz}) = \sum_{k=1}^n \int_{z_k}^{z_{k+1}} (\sigma_{xx}, \sigma_{yy}, \sigma_{xy}, \sigma_{yz}, \sigma_{xz}) dz, \quad (11)$$

$$(M_{xx}, M_{yy}, M_{xy}) = \sum_{k=1}^n \int_{z_k}^{z_{k+1}} (\sigma_{xx}, \sigma_{yy}, \sigma_{xy}) z dz, \quad (12)$$

$$[\bar{C}] = \begin{bmatrix} A & B & 0 \\ B & D & 0 \\ 0 & 0 & A_s \end{bmatrix}, \quad (13)$$

$$(A_{ij}, B_{ij}, D_{ij}) = \sum_{k=1}^n \int_{z_k}^{z_{k+1}} \bar{c}_{ij}^{(k)}(1, z, z^2) dz, \quad (i, j = 1, 2, 3), \quad (14)$$

$$A_{sij} = \beta \sum_{k=1}^n \int_{z_k}^{z_{k+1}} \bar{c}_{ij}^{(k)} dz, \quad (i, j = 4, 5), \quad (15)$$

$$[\bar{e}] = \begin{bmatrix} \bar{e}_{31}^{(1)} & \bar{e}_{31}^{(2)} & \dots & \bar{e}_{31}^{(n)} \\ \bar{e}_{32}^{(1)} & \bar{e}_{32}^{(2)} & \dots & \bar{e}_{32}^{(n)} \\ \bar{e}_{36}^{(1)} & \bar{e}_{36}^{(2)} & \dots & \bar{e}_{36}^{(n)} \\ \bar{e}_{31}^{(1)} \bar{z}^{(1)} & \bar{e}_{31}^{(2)} \bar{z}^{(2)} & \dots & \bar{e}_{31}^{(n)} \bar{z}^{(n)} \\ \bar{e}_{32}^{(1)} \bar{z}^{(1)} & \bar{e}_{32}^{(2)} \bar{z}^{(2)} & \dots & \bar{e}_{32}^{(n)} \bar{z}^{(n)} \\ \bar{e}_{36}^{(1)} \bar{z}^{(1)} & \bar{e}_{36}^{(2)} \bar{z}^{(2)} & \dots & \bar{e}_{36}^{(n)} \bar{z}^{(n)} \\ 0 & 0 & \dots & 0 \\ 0 & 0 & \dots & 0 \end{bmatrix}, \quad (16)$$

$$\bar{z}^{(k)} = (z_k + z_{k+1})/2, \quad (17)$$

$$\{\Delta\phi\} = (\Delta\phi_1, \Delta\phi_2, \dots, \Delta\phi_n)^T, \quad (18)$$

$$\Delta\phi_k = (\phi_{k+1} - \phi_k). \quad (19)$$

Here we have tacitly assumed that $\max(|E_x^{(k)}|, |E_y^{(k)}|) \ll |E_z^{(k)}|$ and neglected contributions of $e_{15}^{(k)} E_y^{(k)}$ and $e_{24}^{(k)} E_x^{(k)}$. It is reasonable because each ply is very thin, which also justifies the assumption that $E_z^{(k)}$ is uniform in the thickness direction. Note that n equals the number of layers, $\beta (= 5/6)$ is the shear correction factor, A , B , and D are 3×3 matrices, and A_s is a 2×2 matrix.

As charge can be collected only in the z -direction, we compute only D_z . Eq. (1b) for the k th ply is:

$$D_z^{(k)} = \bar{e}_{31}^{(k)} \varepsilon_{xx}^{(k)} + \bar{e}_{32}^{(k)} \varepsilon_{yy}^{(k)} + 2\bar{e}_{34}^{(k)} \varepsilon_{xy}^{(k)} + \xi_z^{(k)} E_z^{(k)}. \quad (20)$$

Substitution for $\{\varepsilon\}$ from (6) and for $E_z^{(k)}$ from (7c) into (20) gives:

$$\{\bar{D}_z\} = [\bar{e}]^T \{\bar{\varepsilon}\} + [\bar{\xi}_z] \{\Delta\phi\}, \quad (21)$$

where:

$$\{\bar{D}_z\} = (D_z^{(1)}, D_z^{(2)}, \dots, D_z^{(n)})^T, \quad (22)$$

$$[\bar{\xi}_z] = \begin{bmatrix} \xi_z^{(1)}/(z_2 - z_1) & 0 & \dots & 0 \\ 0 & \xi_z^{(2)}/(z_3 - z_2) & \dots & 0 \\ 0 & 0 & \dots & 0 \\ 0 & 0 & 0 & \xi_z^{(n)}/(z_{n+1} - z_n) \end{bmatrix} \quad (23)$$

The electric enthalpy density, H , for a three-dimensional piezoelectric body including strain energies due to elastic and piezoelectric deformations and the electrical energy is given by [34]:

$$H = \frac{1}{2}\{\varepsilon\}^T[c]\{\varepsilon\} - \{\varepsilon\}^T[e]\{E\} - \frac{1}{2}[E]^T\{\xi\}[E]. \quad (24)$$

For the FSDT, matrices $[c]$ and $[e]$ in (24) are first replaced by $[\bar{c}]$ and $[\bar{e}]$ respectively, and $\{\varepsilon\}$ by the five-dimensional vector obtained from $\{\varepsilon\}$ by deleting ε_{zz} . Substituting for $\{\varepsilon\}$ and $[E]$ from (6) and (7) into (24), and integrating the resulting equation over the plate thickness, we get the following expression for the surface density, H_L , of the electric enthalpy:

$$H_L = \int_{-h/2}^{h/2} H dz = \frac{1}{2}(\{\bar{\varepsilon}\}^T[\bar{C}]\{\bar{\varepsilon}\} - 2\{\bar{\varepsilon}\}^T[\bar{e}]\{\Delta\phi\} - \{\Delta\phi\}^T[\bar{\xi}_z]\{\Delta\phi\}). \quad (25)$$

Equations of motion for the piezoelectric laminate are derived by using the Hamilton principle:

$$\delta \int_0^t dt \int_V \left(\frac{\rho}{2} \{\dot{u}\}^T \{\dot{u}\} - H \right) dV + \int_0^t dt \int_S (\{t\}^T \{\delta u\} - q \delta \phi) dA = 0. \quad (26)$$

Here ρ is the mass/volume, $\{\dot{u}\}^T = (\dot{u}_x, \dot{u}_y, \dot{u}_z)$ is the velocity vector, $\{t\}^T = (t_x, t_y, t_z)$ is the surface traction vector, and q is the charge/surface area. The surface integral in (26) is over all bounding surfaces of the laminate, and V is the volume of the region occupied by the body. Substitutions from (3) and (24) into (26) and integration with respect to z over the plate thickness give:

$$\begin{aligned} & \int_0^t dt \int_{S_0} [\{\delta \dot{U}\}^T [\bar{M}]\{\dot{U}\} - \{\delta \bar{\varepsilon}\}^T [\bar{C}]\{\bar{\varepsilon}\} + \{\delta \bar{\varepsilon}\}^T [\bar{e}]\{\Delta\phi\} \\ & \quad + \{\delta \Delta\phi\}^T [\bar{e}]^T \{\bar{\varepsilon}\} + \{\delta \Delta\phi\}^T [\bar{\xi}_z]\{\Delta\phi\}] dA \\ & + \int_0^t dt \int_{S^\pm} \{\delta U\}^T \{P\} dA - \int_{S^\pm} \{\delta \phi\}^T \{q\} dA = 0, \end{aligned} \quad (27)$$

where

$$\{U\} = (u_0 \ v_0 \ \psi_x \ \psi_y \ w_0)^T, \quad (28)$$

$$[\bar{M}] = \begin{bmatrix} I_0 & 0 & I_1 & 0 & 0 \\ 0 & I_0 & 0 & I_1 & 0 \\ I_1 & 0 & I_2 & 0 & 0 \\ 0 & I_1 & 0 & I_2 & 0 \\ 0 & 0 & 0 & 0 & I_0 \end{bmatrix}, \quad (29)$$

$$(I_0, I_1, I_2) = \sum_{k=1}^n \int_{z_k}^{z_{k+1}} \rho^{(k)}(1, z, z^2) dz, \quad (30)$$

I_0, I_1, I_2 are the normal, coupled normal-rotary, and rotary inertia coefficients, respectively. $\{U\}$ is the vector of generalized displacements, $\{P\}$ is the vector of generalized surface tractions conjugate to $\{U\}$, S_0 is the midsurface of

the plate, and S^+ and S^- are, respectively, the top and the bottom surfaces of the plate.

Eq. (27) can be viewed as a weak formulation of equations governing electromechanical deformations of the hybrid piezoelectric plate.

III. FINITE-ELEMENT FORMULATION

The midsurface of the plate is divided into eight-node isoparametric quadrilateral elements. The same set of shape functions is used to approximate the electric potential, and each one of the five components of the generalized displacement. That is:

$$\{U(x, y, t)\} = [N_U(x, y)]\{U^e(t)\}, \quad (31a)$$

$$\{\phi(x, y, t)\} = [N_\phi(x, y)]\{\phi^e(t)\}, \quad (31b)$$

where:

$$\begin{aligned} [N_U(x, y)] &= [N_1(x, y)I_u, N_2(x, y)I_u, \dots, N_8(x, y)I_u], \\ [N_\phi(x, y)] &= [N_1(x, y)I_\phi, N_2(x, y)I_\phi, \dots, N_8(x, y)I_\phi], \end{aligned} \quad (32)$$

here I_u and I_ϕ are, respectively, 5×5 and $n \times n$ identity matrices, and $\{U^e(t)\}$ and $\{\phi^e(t)\}$ are 40×1 and $8n \times 1$ matrices, respectively. Substitution from (28), (6), and (31a) into (10) yields:

$$\{\bar{\varepsilon}\} = [B_U]\{U^e\}, \quad (33)$$

where:

$$[B_{U_i}] = \begin{bmatrix} N_{i,x} & 0 & 0 & 0 & 0 \\ 0 & N_{i,y} & 0 & 0 & 0 \\ N_{i,y} & N_{i,x} & 0 & 0 & 0 \\ 0 & 0 & N_{i,x} & 0 & 0 \\ 0 & 0 & 0 & N_{i,y} & 0 \\ 0 & 0 & N_{i,y} & N_{i,x} & 0 \\ 0 & 0 & 0 & N_i & N_{i,y} \\ 0 & 0 & N_i & 0 & N_{i,x} \end{bmatrix}, \quad i = 1, 2, \dots, 8, \quad (34)$$

$$N_{i,x} = \partial N_i / \partial x \text{ etc.}, \quad (35)$$

$$[B_U] = [B_{U1} \ B_{U2} \ \dots \ B_{U8}]. \quad (36)$$

Similarly:

$$\{\Delta\phi\} = -[B_\phi]\{\phi^e\}, \quad (37)$$

where:

$$[B_\phi] = \begin{bmatrix} 1 & 0 & \dots & 0 & 0 \\ -1 & 1 & \dots & 0 & 0 \\ \dots & \dots & \dots & \dots & \dots \\ 0 & 0 & \dots & -1 & 1 \end{bmatrix}_{n \times n} [N_\phi]_{n \times 8n}. \quad (38)$$

Substitution from (31), (33), and (37) into (27) and exploiting the fact that the resulting equation must hold for all choices of δU and $\delta \Delta\phi$ that vanish where U and ϕ are prescribed, we obtain the following two equations

governing the time evolution of the generalized nodal displacements and the nodal electric potentials:

$$[M]\{\ddot{U}\} + [K_{UU}]\{U\} + [K_{U\phi}]\{\phi\} = \{F\}, \quad (39)$$

$$[K_{\phi U}]\{U\} + [K_{\phi\phi}]\{\phi\} = \{G\}, \quad (40)$$

where:

$$[M] = \sum_e \int_{S_e} [N_U]^T [\bar{M}] [N_U] dA, \quad (41)$$

$$[K_{UU}] = \sum_e \int_{S_e} [B_U]^T [\bar{C}] [B_U] dA, \quad (42)$$

$$[K_{U\phi}] = \sum_e \int_{S_e} [B_U]^T [\bar{e}] [B_\phi] dA, \quad (43)$$

$$[K_{\phi U}] = [K_{U\phi}]^T, \quad (44)$$

$$[K_{\phi\phi}] = - \sum_e \int_{S_e} [B_\phi]^T [\bar{\xi}_z] [B_\phi] dA, \quad (45)$$

$$\{F\} = \sum_e \int_{S_e^\pm} [N_U]^T \{P\} dA, \quad (46)$$

$$\{G\} = - \sum_e \int_{S_e^\pm} [N_\phi]^T \{q\} dA. \quad (47)$$

The summation in (41)–(47) is over all elements. Eq. (39) and (40) can be written as:

$$\begin{bmatrix} M & 0 \\ 0 & 0 \end{bmatrix} \begin{Bmatrix} \ddot{U} \\ \ddot{\phi} \end{Bmatrix} + \begin{bmatrix} K_{UU} & K_{U\phi} \\ K_{\phi U} & K_{\phi\phi} \end{bmatrix} \begin{Bmatrix} U \\ \phi \end{Bmatrix} = \begin{Bmatrix} F(t) \\ G(t) \end{Bmatrix}. \quad (48)$$

The electric potential on the faces of PZT layers that act as sensors is grouped together into the array $\{\phi^S\}$, and on those acting as actuators into the array $\{\phi^A\}$. Eq. (48) is split into the following two equations:

$$[M]\{\ddot{U}\} + [K_{UU}]\{U\} + [K_{U\phi}^{SS}]\{\phi^S\} = \{F\} - [K_{U\phi}^{SA}]\{\phi^A\}, \quad (49a)$$

$$[K_{\phi U}^{SS}]\{U\} + [K_{\phi\phi}^{SS}]\{\phi^S\} = \{G\} - [K_{\phi\phi}^{SA}]\{\phi^A\}, \quad (49b)$$

where superscripts S and A indicate partitioned submatrices. Substitution for ϕ^S from (49b) into (49a) gives a set of coupled ordinary differential equations for the determination of U . These equations subject to the prescribed initial displacements, initial velocities, and boundary conditions are integrated with respect to time t . Having found U , ϕ^S can be computed from (49b).

For free vibrations of the hybrid plate $\{F\} = \{0\}$, $\{G\} = \{0\}$, and one assumes that:

$$\{U(t)\} = \{\tilde{U}\}e^{i\omega t}, \quad \{\phi(t)\} = \{\tilde{\phi}\}e^{i\omega t}, \quad (50)$$

where ω is a natural frequency, and \tilde{U} and $\tilde{\phi}$ are, respectively, amplitudes of the displacement and the electric potential. Substitution from (50) into (48) and setting $\{F\} = \{0\}$, $\{G\} = \{0\}$, we get:

$$\begin{bmatrix} K_{UU} & K_{U\phi} \\ K_{\phi U} & K_{\phi\phi} \end{bmatrix} \begin{Bmatrix} \tilde{U} \\ \tilde{\phi} \end{Bmatrix} = \omega^2 \begin{bmatrix} M & 0 \\ 0 & 0 \end{bmatrix} \begin{Bmatrix} \tilde{U} \\ \tilde{\phi} \end{Bmatrix}, \quad (51)$$

or:

$$[\tilde{K}]\{\tilde{U}\} = \omega^2 [M]\{\tilde{U}\}, \quad (52)$$

where:

$$[\tilde{K}] = [K_{UU}] - [K_{U\phi}][K_{\phi\phi}]^{-1}[K_{\phi U}]. \quad (53)$$

The second term on the right-hand side of (53) describes the effect of electromechanical coupling on the natural frequencies of the hybrid plate.

Mechanical boundary conditions imposed at clamped (C), free (F), and simply supported (SP) edges are given below.

$$\begin{aligned} \text{C: } & u_0 = v_0 = w_0 = \psi_x = \psi_y = 0; \\ \text{F: } & N_{xx} = N_{xy} = Q_{xz} = M_{xx} = M_{xy} = 0 \text{ on } x = 0, a, \\ & N_{yy} = N_{xy} = Q_{yz} = M_{yy} = M_{yx} = 0 \text{ on } y = 0, b; \\ \text{SP: } & w_0 = 0, N_{xx} = N_{xy} = M_{xx} = M_{xy} = 0 \text{ on } x = 0, a, \\ & w_0 = 0, N_{yy} = N_{xy} = M_{yy} = M_{yx} = 0 \text{ on } y = 0, b. \end{aligned} \quad (54)$$

Electrical boundary conditions for grounded (or short-circuit) and open-circuited layers are:

$$\text{Grounded: } \phi = 0,$$

$$\text{Open-Circuited: } D_z = 0 \text{ on the surface } z = \text{const.}$$

IV. RESULTS AND DISCUSSION

A. Static Deformations

1. *Comparison of Computed Results with Experimental Observations of Crawley and Lazarus:* A computer code based on the afore-stated formulation has been developed. It uses an eight-node isoparametric element and 2×2 integration rule. It has been verified and validated by analyzing the problem studied experimentally by Crawley and Lazarus [1]. The 0.83-mm thick $[0/\pm 45^\circ]_s$ AS4/3501 graphite/epoxy cantilever plate has 15 PZT-4 patches bonded symmetrically to its top and bottom surfaces as shown in Fig. 2 in which dimensions of the plate also are given. An electric field of 395 V/mm of opposite polarity is applied to PZTs bonded to the top and the bottom surfaces of the plate. The graphite/epoxy is modeled as an orthotropic material and the PZT as transversely isotropic with the z -axis as the axis of transverse isotropy. Values of material parameters are listed in Table I. Fig. 3 compares the computed and the observed transverse deflections T_1 , T_2 , and T_3 normalized as follows:

$$T_1 = w_2/b,$$

$$T_2 = (w_2 - 0.5(w_1 + w_3))/b,$$

$$T_3 = (w_3 - w_1)/b$$

Here w_2 , w_1 , and w_3 are, respectively, the transverse displacement of a point on the centroidal axis and the left

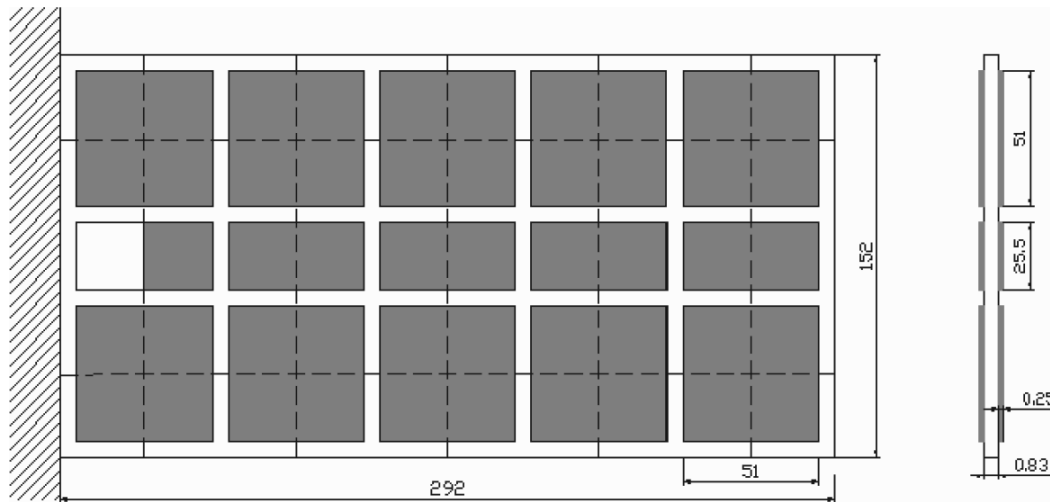


Fig. 2. Cantilever composite plate with surface-bonded piezoelectric actuators [1].

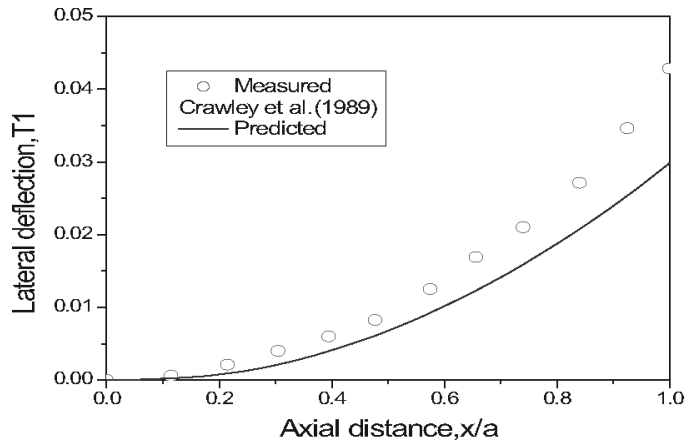
TABLE I
MATERIAL PROPERTIES (ELECTRIC PERMITTIVITY OF AIR, $\epsilon_0 = 8.85 \times 10^{-12}$ F/m).

Property	0° AS4/3501	PZT-4	0° T300/976	PZT G1195N
Elastic properties:				
E_{11} (GPa)	132.38	81.3	150.0	63.0
E_{22} (GPa)	10.76	81.3	9.0	63.0
E_{33} (GPa)	10.76	64.5	9.0	63.0
G_{23} (GPa)	3.61	25.6	2.5	24.2
G_{13} (GPa)	5.65	25.6	7.1	24.2
G_{12} (GPa)	5.65	30.6	7.1	24.2
ν_{12}	0.24	0.33	0.3	0.3
ν_{13}	0.24	0.43	0.3	0.3
ν_{23}	0.49	0.43	0.3	0.3
Piezoelectric Coefficients (10^{-12} m/V)				
e_{31}	0	122.0	0	254.0
e_{32}	0	122.0	0	254.0
e_{33}	0	285.0	0	374.0
e_{24}	0	0	0	584.0
e_{15}	0	0	0	584.0
Electric permittivity				
ξ_{11}/ϵ_0	3.5	1475.0	3.5	1728.8
ξ_{22}/ϵ_0	3.0	1475.0	3.0	1728.8
ξ_{33}/ϵ_0	3.0	1300.0	3.0	1694.9
Mass density ρ (kg/m ³)	1578.0	7600.0	1600	7600

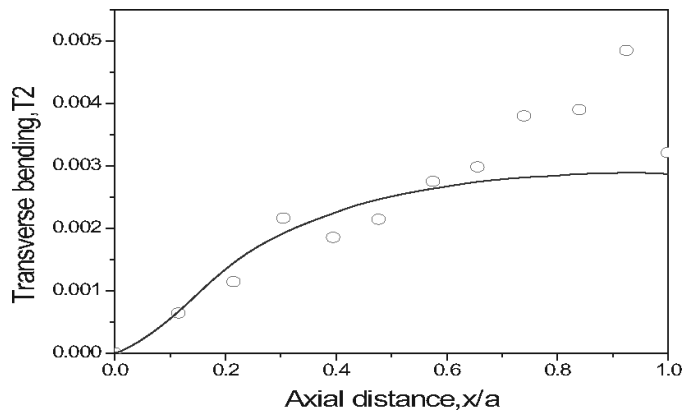
edge and the right edge of the midsurface of the plate, and b is the plate width. The normalized displacements T_1 , T_2 , and T_3 represent, respectively, the bending deflection of the centroidal axis, the transverse bending curvature, and the twisting angle due to the coupling between bending and twisting. Results have been computed by neglecting the effect of inertia forces. It is clear that the computed transverse deflection of a point on the centroidal axis agrees well with the measured one. However, the agreement between the computed and the measured deflections of points on an edge of the plate is not very good. This discrepancy could be due to the three-dimensional effects present at points near the free edges of the plate that are

ignored in the FSDT. These effects are negligible at points on the centroidal axis.

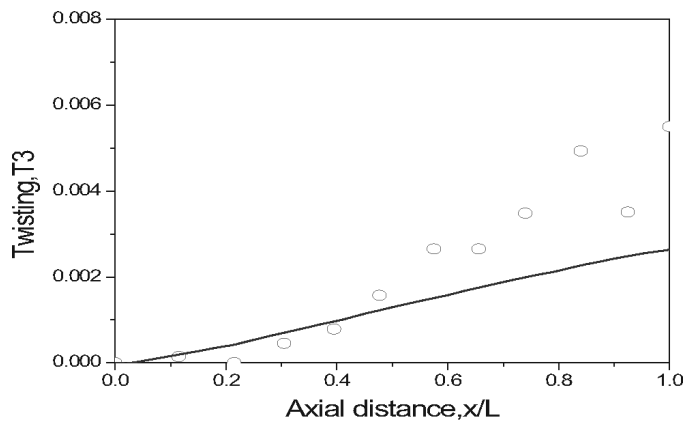
2. *Deflection of a Hybrid Plate with PZT Layers Grounded Versus Short Circuited:* We now investigate the effect boundary conditions imposed on PZT layers have on the lateral deflections of a plate subjected to mechanical loads. Two problems, namely a cantilever plate and a simply supported plate each made of a single 0° AS4/3501 graphite/epoxy layer with identical G-1195N (Piezo System, Cambridge, MA) PZT layers bonded to its entire top and bottom surfaces are analyzed; the plate geometry is shown in Fig. 4(a). The hybrid cantilever plate is loaded



(a)

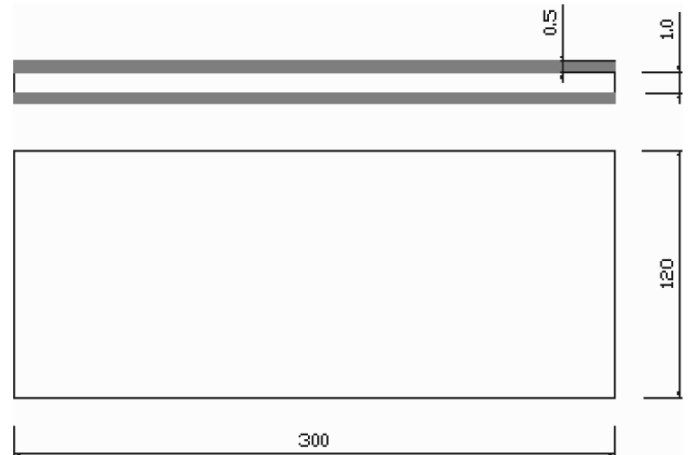


(b)

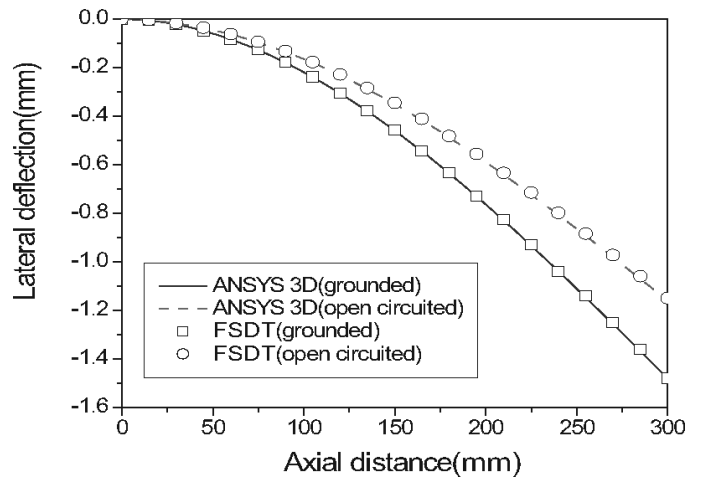


(c)

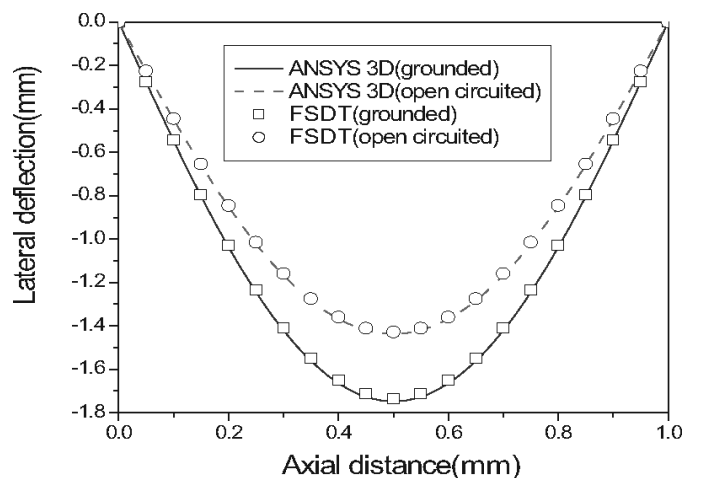
Fig. 3. Comparison of the computed transverse deflections with the test values of [1]. (a) Transverse deflection of the centroidal axis, (b) the transverse bending curvature, and (c) the transverse twisting angle.



(a)



(b)



(c)

Fig. 4. (a) Composite laminated plate with surface-bonded piezoelectric layers (dimensions in mm). (b) Comparison of transverse deflections of the centroidal axis computed from the present code with those from the three-dimensional commercial code ANSYS; cantilever. (c) Simply supported only on the left and the right edges.

TABLE II
LAY-UP OF LAYERS: [0/-0/0/-0/PIC151/-0/0/-0/0].

Mode No.	Exp.	ANSYS	% Error	Present code	% Error	Mode Shapes
1	961	899.73	-6.38	896.5	-6.71	
2	1073	1015	-5.41	1025.7	-4.41	
3	2158	2097	-2.83	2090.7	-3.12	
4	2837	2786.4	-1.78	2800.9	-1.27	
5	—	3908	—	3892.6	—	
6	4361	4023.7	-7.73	4004.4	-8.18	
7	4729	4416.1	-6.62	4390.2	-7.16	
8	5525	5364.8	-2.90	5341.2	-3.33	
9	5950	5640.6	-5.20	5601.7	-5.85	
10	—	—	—	—	—	
11	6529	6508.6	-0.31	6453.2	-1.16	
12	7461	7375.1	-1.15	7284.9	-2.36	
13	9018	8957.1	-0.68	8844.7	-1.92	








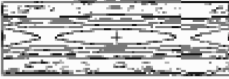





by a 10 N/m uniformly distributed load on its free edge and the simply supported hybrid plate by 1 kN/m² uniformly distributed pressure on its top surface. In each case, effects of inertial forces are neglected. Three-dimensional deformations of each problem also are analyzed with the commercial code ANSYS by dividing the graphite/epoxy layer into $50 \times 20 \times 2$ eight-node (solid 45) brick elements, and each piezoceramic layer into $50 \times 20 \times 1$ eight-node coupled field (solid 5) brick elements. For analysis with the present code based on the FSDT theory, the plate is divided into 50×20 eight-node isoparametric quadrilateral elements. It is clear from the results depicted in Figs. 4(b) and (c) that the two deflected shapes of the centroidal axis of the plate agree with each other. Also plotted in Figs. 4(b) and (c) are the deflected shapes when the PZT

layers are open circuited (i.e., act as sensors) and when they are grounded. Because the PZT layers also store electric energy in the former case, it should deflect less than that when these layers are grounded. The difference in the tip deflections of the cantilever plate computed with grounded and open-circuited PZT layers is 21.6%. The two deflections of the centroid of the simply supported plate differ by 17.8%. These differences in deflections illustrate the importance of considering proper boundary conditions on the PZT layers.

B. Natural Frequencies

1. *Comparison with Experimental Results:* For five different orientations of plies in a nine-layer hybrid lami-

TABLE III
LAY-UP OF LAYERS: [30/-30/30/-30/PIC151/-30/30/-30/30].






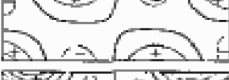







Mode No.	Exp.	ANSYS	% Error	Present code	% Error	Mode Shapes
1	848	751.08	-11.43	746.09	-12.02	
2	1473	1334.7	-9.39	1316.3	-10.64	
3	2249	2110.9	-6.14	2090.6	-7.04	
4	3064	2829	-7.67	2785	-9.11	
5	4314	3957.7	-8.26	3895.7	-9.70	
6	4660	4468.2	-4.12	4388.3	-5.83	
7	5012	4799.7	-4.24	4719.9	-5.83	
8	5415	—	—	—	—	
9	5730	5034.3	-12.14	4930.6	-13.95	
10	6960	6639.3	-4.61	6496.4	-6.66	
11	—	7013.6	—	6837.6	—	
12	7531	7355.2	-2.33	7204.9	-4.33	
13	—	9409.4	—	9157.3	—	

nated plate with all edges free, we have compared in Tables II–VI the presently computed first 13 natural frequencies with the experimental values of [33]. Material properties and dimensions of the plate are given in [33]. We also have included in Tables II–VI frequencies computed with the three-dimensional, finite-element code ANSYS, and depicted the mode shape obtained from the present code. A dash signifies that this frequency was either not observed in experiments or not computed from the code. The frequency corresponding to mode shape 10 in Table II could neither be computed with the present code nor observed experimentally. However, Lin *et al.* [33] computed this mode with ANSYS by using their FEM I and FEM II formulations. Frequencies computed with ANSYS essentially equal those listed in Tables IV through VIII of [33] under the column FEM III because the two analyses used

the same solid elements in ANSYS. The percent error between the experimental frequency and that computed by the present code is nearly the same as that between the test value and the value obtained from ANSYS. The two percentage errors differ by at most 2%. However, the maximum difference between the computed and the experimental frequency is ~15%. In summary, for all five hybrid plates, the first 10 frequencies computed from the FSDT differ at most by ~15% from their corresponding experimental values, and by ~2% from those computed with ANSYS. The first 13 modes of vibration of the five plates are compared in Fig. 5.

2. *Frequencies of a Hybrid Plate with PZT Layers Grounded Versus Open Circuited:* For the cantilever and the simply supported plates studied in Section IV-B and

TABLE IV
LAY-UP OF LAYERS: [45/-45/45/-45/PIC151/-45/45/-45/45].

Mode No.	Exp.	ANSYS	% Error	Present code	% Error	Mode Shapes
1	648	578.43	-10.74	573.41	-11.51	
2	1471	1427.6	-2.95	1407.3	-4.33	
3	1746	1658.8	-4.99	1641.6	-5.98	
4	2983	2954.2	-0.97	2906.4	-2.57	
5	3510	3288.1	-6.32	3246.1	-7.52	
6	4687	4658.4	-0.61	4568.5	-2.53	
7	—	5246	—	5153.8	—	
8	5496	5301.7	-3.54	5218.4	-5.05	
9	6388	6229.9	-2.47	6113.9	-4.29	
10	6736	6784.5	0.72	6633	-1.53	
11	7698	7658.1	-0.52	7469.6	-2.97	
12	8439	8594.8	1.85	8404.3	-0.41	
13	9083	9228.5	1.60	8991.4	-1.01	

using the same FE meshes as those described there, we have listed in Table VII the first 10 natural frequencies computed with the present code and with ANSYS for the faces of the two PZT layers either grounded or open circuited. In each case, the first natural frequency computed with the present code agrees very well with that obtained from ANSYS. However, the difference between frequencies computed with the two codes increases with an increase in the order of the mode shape. Also, the open circuited and the grounded PZT layers give quite different frequencies; the first natural frequency in the two cases differs by 14.2% for the cantilever plate and 9.4% for the simply supported plate.














3. Frequencies of a Hybrid Plate with Two Opposite Edges Clamped: For the hybrid plates analyzed in Sec-

tion IV-B,1, we have listed in Table VIII the first 13 frequencies computed with the present code when edges $x = 0$ and $x = 70$ mm are clamped and the other two are free. The PZT faces are open-circuited. A comparison of frequencies listed in Tables II and VIII reveals that clamping these two edges increases each one of the first 13 frequencies; the maximum percent increase is $\sim 14\%$.

C. Piezoelectric Layers Acting as Sensors

Static deformations of a hybrid composite plate comprised of $[0/\pm 45^\circ]$ T300/976 graphite/epoxy (DuPont, Wilmington, DE) plate with four G1195N PZT patches bonded symmetrically to its top and bottom surfaces as shown in Fig. 6(a) are studied. All PZT layers act as sensors, and the plate is loaded by a uniformly distributed

TABLE V
LAY-UP OF LAYERS: [60/-60/60/-60/PIC151/-60/60/-60/60].

Mode No.	Exp.	ANSYS	% Error	Present code	% Error	Mode Shapes
1	596	510.77	-14.30	505.89	-15.12	
2	1281	1304.4	1.83	1286.1	0.40	
3	1517	1434.6	-5.43	1419	-6.46	
4	2673	2693.3	0.76	2650.4	-0.85	
5	3048	2844.2	-6.69	2808.7	-7.85	
6	4143	4244	2.44	4164.1	0.51	
7	4877	4712.3	-3.38	4643.6	-4.79	
8	5924	6015.3	1.54	5882.1	-0.71	
9	6524	6364.8	-2.44	6263	-4.00	
10	7087	7006.7	-1.13	6878.3	-2.94	
11	—	7232.7	—	7107.5	—	
12	—	8084.1	—	7878.8	—	
13	8479	8560.6	0.96	8359.8	-1.41	

pressure of 1 N/m². The cantilever plate is clamped at the left edge. The left and the right edges of the other plate are simply supported, and the other two edges are free. The thickness of the hybrid plate is not uniform. The computed electric potentials on top surfaces of the upper PZT patches are depicted in Figs. 6(b) and (c). In each case, the maximum voltage occurs at points of the maximum curvature.

V. CONCLUSIONS

We have used a coupled electromechanical theory to analyze static deformations and free vibrations of a hybrid laminated rectangular plate comprised of PZT layers or

patches either embedded in or bonded to outer surfaces of graphite/epoxy plies. A FSDT and a finite-element code using eight-node isoparametric elements have been developed. It is shown that the FSDT gives results close to those obtained from the three-dimensional commercial code ANSYS. Computed results show that the tip deflection of a hybrid cantilever plate and the centroidal deflection of a plate simply supported on two opposite edges with open circuited PZT layers are, respectively, 21.6% and 17.8% less than those when the PZT layers are grounded. The natural frequencies of the two plates differ by 14.2% and 9.4% for the two sets of boundary conditions on the PZT layers. Thus, one should use a coupled electromechanical theory in designing a precision equipment such as a bimorph.

TABLE VI
LAY-UP OF LAYERS: [90/-90/90/-90/PIC151/-90/90/-90/90].

Mode No.	Exp.	ANSYS	% Error	Present code	% Error	Mode Shapes
1	615	510.68	-16.96	505.25	-17.85	
2	926	877.81	-5.20	861.68	-6.95	
3	1539	1407.6	-8.54	1391.1	-9.61	
4	1932	1862.1	-3.62	1826.3	-5.47	
5	3096	2757.5	-10.93	2721.4	-12.10	
6	3234	3051.1	-5.66	2988.9	-7.58	
7	4733	4531.3	-4.26	4433.1	-6.34	
8	5037	4550.4	-9.66	4483.1	-11.00	
9	—	—	—	—	—	
10	6765	6368.4	-5.86	6221.7	-8.03	
11	7231	6770.8	-6.36	6658.6	-7.92	
12	7841	7961.4	1.54	7812.6	-0.36	
13	8106	8122.2	0.20	7965.5	-1.73	

TABLE VII
COMPARISON OF NATURAL FREQUENCIES (Hz) COMPUTED FROM THE PRESENT FSDT FORMULATION WITH THOSE FROM THE THREE-DIMENSIONAL COMMERCIAL CODE ANSYS.

Mode No.	Cantilever laminated plate				Laminated plate with the left and right edges simply supported			
	grounded		open-circuit		grounded		open-circuit	
	ANSYS	FSDT	ANSYS	FSDT	ANSYS	FSDT	ANSYS	FSDT
1	16.09	16.09	18.38	18.466	44.37	44.48	48.52	48.625
2	76.67	77.00	78.50	79.068	142.02	143.11	144.2	145.44
3	100.4	101.27	113.38	114.72	179.52	181.96	201.15	204.43
4	246.7	249.12	256.63	260.4	324.9	328.58	340.28	345.62
5	292.12	289.05	319.56	328.81	407.39	420.27	465.11	483.4
6	464.27	473.72	494.4	508.75	575.62	588.55	620.23	640.91
7	550.7	575.54	620.08	650.58	667.81	682.21	835.12	846.95
8	620	637.62	769.78	794.74	728.66	770.22	841.76	901.74
9	752.35	775.54	818.12	868.94	851.74	870.51	998.89	1037
10	755.69	781.16	889.23	885.82	907.83	946.74	1023.4	1061.7

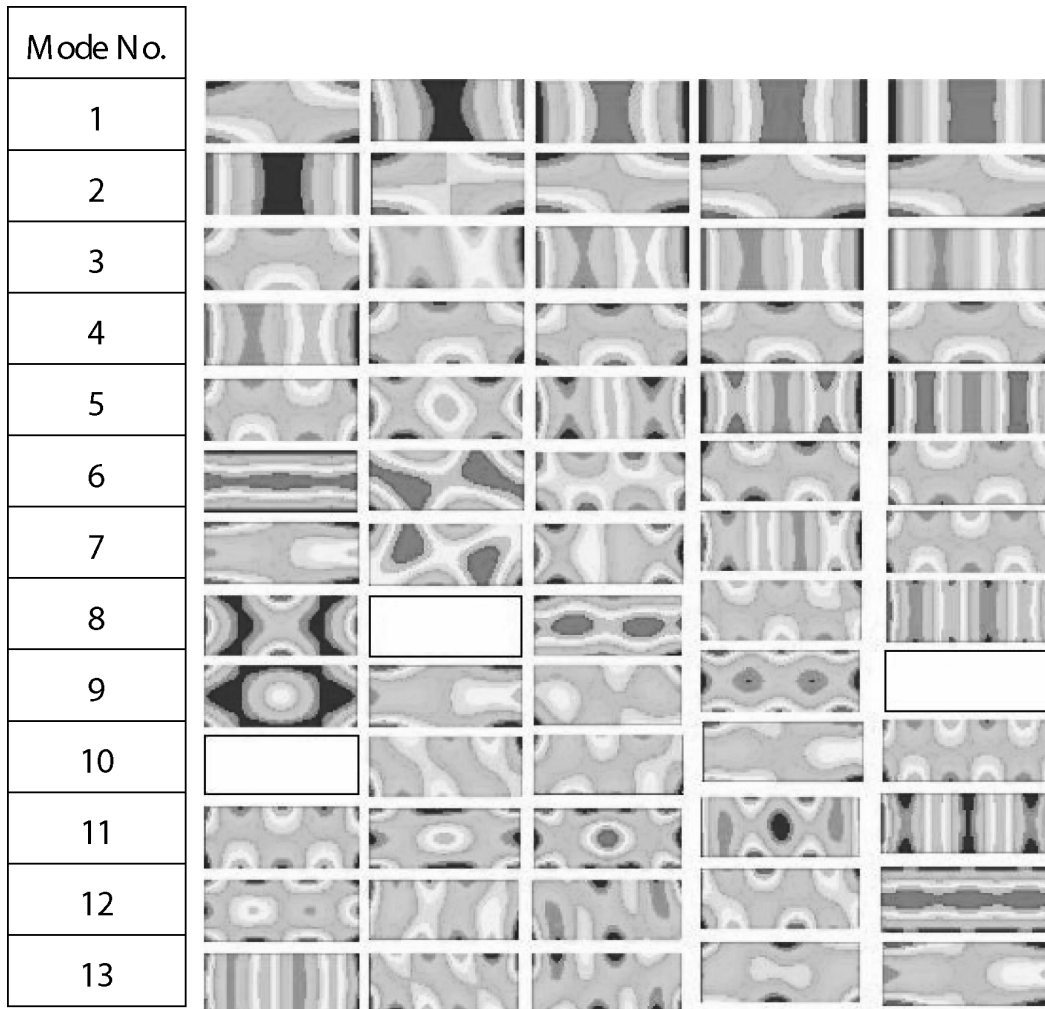


Fig. 5. Comparison of modes of vibration of a hybrid plate with the five different orientation of fibers listed in Tables II–VI. Figures in columns 2, 3, 4, 5, and 6 are, respectively, for the plates of Tables II–VI.

TABLE VIII

FREQUENCIES COMPUTED WITH THE PRESENT CODE FOR A HYBRID LAMINATED PLATE WITH THE LEFT AND RIGHT EDGES CLAMPED AND THE OTHER TWO FREE. ALL EDGES ARE OPEN-CIRCUITED.

A^1	B	C	D	E
938.95	785.76	623.87	528.42	503.81
1260.3	1535.9	1556.8	1417.4	1023.9
2499.3	2119.9	1701.1	1442.4	1374.9
2961.9	3288.5	3208.1	2800.5	2211.2
4182.6	4054.6	3329.5	2944.2	2662.3
4700.3	5061.7	5115.6	4562.8	3663.1
5207.3	5382.3	5384.9	4669.2	4335.9
5503.1	6486.5	5877.8	6578.2	5419.5
6474.3	6884.5	7299.4	6741.4	6103.4
7408.8	7841.1	7587.8	6807.8	6366.7
7521.2	8649.9	7840.5	7731.6	7484.8
7927.2	9239	8416.9	8075.8	7716.4
10081	9345.9	9763.9	8801.7	8314.6

$^1 A = [0/0/0/0/p0/0/0/0/0]$,
 $B = [-30/30/-30/30/p0/30/-30/30/-30]$,
 $C = [-45/45/-45/45/p0/45/-45/45/-45]$,
 $D = [-60/60/-60/60/p0/60/-60/60/-60]$,
 $E = [-90/90/-90/90/p0/90/-90/90/-90]$,

REFERENCES

- [1] E. F. Crawley and K. B. Lazarus, "Induced strain actuation of composite plate," presented at 30th AIAA Structural Dynamics and Mater. Conf., Mobile, AL, 1989.
- [2] E. F. Crawley and J. de Luis, "Use of piezoelectric actuators as element of intelligent structures," presented at 27th AIAA/ASME/ASCE/AHS Structures, Structural Dynamics and Mater. Conf., San Antonio, TX, 1987.
- [3] B. T. Wang and C. A. Rogers, "Laminate plate theory for distributed induced strain actuators," *J. Composite Mater.*, vol. 25, pp. 433–452, 1991.
- [4] L. Yao, L. Lu, Z. H. Wang, W. G. Zhu, and Y. Dai, "Exact solution of multilayered piezoelectric diaphragms," *IEEE Trans. Ultrason., Ferroelect., Freq. Contr.*, vol. 50, pp. 1262–1271, 2003.
- [5] D. K. Shah, S. P. Joshi, and W. S. Chan, "Static structural response of plates with piezoelectric layers," *Smart Mater. Struct.*, vol. 2, pp. 172–180, 1993.
- [6] K. Ghosh and R. C. Batra, "Shape control of plates using piezoelectric elements," *AIAA J.*, vol. 33, no. 7, pp. 1354–1357, 1995.
- [7] K. Ghosh and R. C. Batra, "Shape control of plates using piezoceramic elements," *Proc. SPIE*, vol. 2427, pp. 107–121, 1995.
- [8] R. C. Batra and K. Ghosh, "Deflection control during dynamic deformations of a rectangular plate using piezoceramic elements," *AIAA J.*, vol. 33, pp. 1547–1548, 1995.
- [9] K. Chandrashekhara and K. Bhatia, "Active buckling control of smart composite plates—finite element analysis," *Smart Mater. Struct.*, vol. 2, pp. 31–39, 1993.

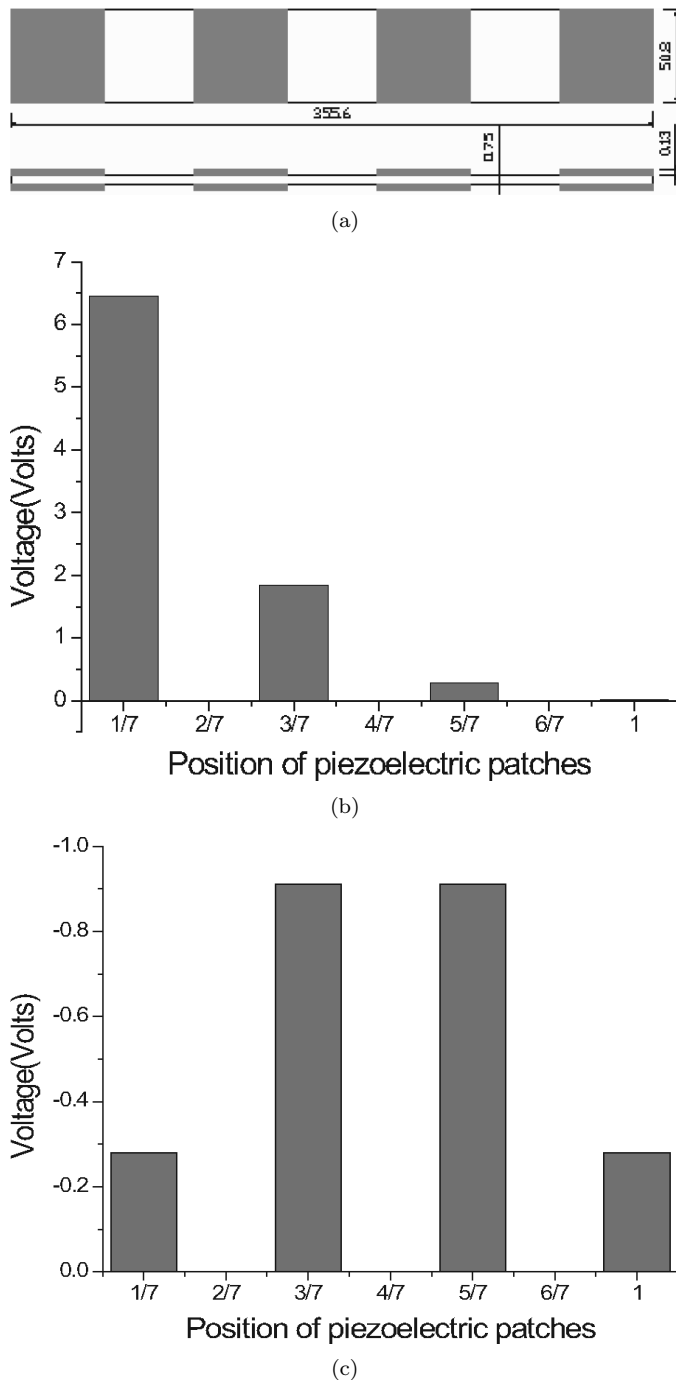


Fig. 6. (a) Composite plate T399/976[0/±45]_s with surface-bonded distributed piezoelectric sensors. Computed voltage of sensors (b) cantilever plate (left end fixed); (c) only the left and right edges simply supported.

- [10] K. Chandrashekhara and R. Tenneti, "Thermally induced vibration suppression of laminated plates with piezoelectric sensors and actuators," *Smart Mater. Struct.*, vol. 4, pp. 281–290, 1995.
- [11] S. Varadarajan, K. Chandrashekhara, and S. Agarwal, "Adaptive shape control of laminated composite plates using piezoelectric materials," *AIAA J.*, vol. 36, no. 9, pp. 1694–1698, 1998.
- [12] H. Allik and T. J. R. Hughes, "Finite element method for piezoelectric vibration," *Int. J. Numer. Methods Eng.*, vol. 2, pp. 151–157, 1970.
- [13] R. C. Batra and X. Q. Liang, "Finite dynamic deformations of smart structures," *Comp. Mechs.*, vol. 20, pp. 427–438, 1997.
- [14] R. C. Batra and T. S. Geng, "Enhancement of the dynamic buckling load for a plate by using piezoceramic actuators," *Smart Mater. Struct.*, vol. 10, pp. 925–933, 2001.
- [15] R. C. Batra and T. S. Geng, "Comparison of active constrained layer damping by using extension and shear mode actuators," *J. Intelligent Mater. Struct.*, vol. 13, no. 6, pp. 349–367, 2002.
- [16] S. K. Ha, C. Keilers, and F. K. Chang, "Finite element analysis of composite structures containing distributed piezoceramic sensors and actuators," *AIAA J.*, vol. 30, no. 3, pp. 772–780, 1992.
- [17] J. Kim, V. V. Varadan, V. K. Varadan, and X. Q. Bao, "Finite element modeling of a smart cantilever plate and comparison with experiments," *Smart Mater. Struct.*, vol. 5, pp. 165–170, 1996.
- [18] Y. H. Lim, S. V. Gopinathan, V. V. Varadan, and V. K. Varadan, "Finite element simulation of smart structures using an optimal output feedback controller for vibration and noise control," *Smart Mater. Struct.*, vol. 8, pp. 324–337, 1999.
- [19] D. A. Saravanos, P. R. Heyliger, and D. A. Hopkins, "Layerwise mechanics and finite element for the dynamic analysis of piezoelectric composite plates," *Int. J. Solids Struct.*, vol. 34, no. 3, pp. 359–378, 1997.
- [20] R. P. Thornburgh and A. Chattopadhyay, "Nonlinear actuation of smart composite using a coupled piezoelectric-mechanical model," *Smart Mater. Struct.*, vol. 10, pp. 743–749, 2001.
- [21] S. Vidoli and R. C. Batra, "Derivation of plate and rod equations for a piezoelectric body from a mixed three-dimensional variational principle," *J. Elasticity*, vol. 59, pp. 23–50, 2000.
- [22] J. S. Yang and R. C. Batra, "Mixed variational principles in nonlinear piezoelectricity," *Int. J. Nonlinear Mech.*, vol. 30, pp. 719–726, 1995.
- [23] R. C. Batra and S. Vidoli, "Higher order piezoelectric plate theory derived from a three-dimensional variational principle," *AIAA J.*, vol. 40, no. 1, pp. 91–104, 2002.
- [24] S. S. Vel and R. C. Batra, "Analysis of piezoelectric bimorphs and plates with segmented actuators," *J. Thin-Walled Struct.*, vol. 39, no. 1, pp. 23–44, 2001.
- [25] S. S. Vel and R. C. Batra, "Three-dimensional analytical solutions for hybrid multilayered piezoelectric plates," *J. Appl. Mech.*, vol. 67, pp. 558–567, 2000.
- [26] S. S. Vel, R. Mewer, and R. C. Batra, "Analytical solution for the cylindrical bending vibration of piezoelectric composite plates," *Int. J. Solids Struct.*, vol. 41, pp. 1625–1643, 2004.
- [27] J. S. Yang, R. C. Batra, and X. Q. Liang, "The cylindrical bending vibrations of a laminated elastic plate due to piezoelectric actuators," *Smart Mater. Struct.*, vol. 3, pp. 485–493, 1994.
- [28] R. C. Batra, X. Q. Liang, and J. S. Yang, "Shape control of vibrating simply supported plates," *AIAA J.*, vol. 34, pp. 116–122, 1996.
- [29] R. C. Batra, X. Q. Liang, and J. S. Yang, "The vibration of a simply supported rectangular elastic plate due to piezoelectric actuators," *Int. J. Solids Struct.*, vol. 33, pp. 1597–1618, 1996.
- [30] S. Vidoli and R. C. Batra, "Coupled extensional and torsional deformations of a piezoelectric cylinder," *Smart Mater. Struct.*, vol. 10, pp. 300–304, 2001.
- [31] S. S. Vel and R. C. Batra, "Exact solution for the cylindrical bending of laminated plates with embedded shear actuators," *Smart Mater. Struct.*, vol. 10, pp. 240–251, 2001.
- [32] S. S. Vel and R. C. Batra, "Exact solution for rectangular sandwich plates with embedded piezoelectric shear actuators," *AIAA J.*, vol. 39, pp. 1363–1373, 2001.
- [33] H. Y. Lin, J. H. Huang, and C. C. Ma, "Vibration analysis of angle-ply laminated composite plates with an embedded piezoceramic layer," *IEEE Trans. Ultrason., Ferroelect., Freq. Contr.*, vol. 50, no. 9, pp. 1084–1099, 2003.

- [34] H. F. Tiersten, *Linear Piezoelectric Plate Vibrations*. New York: Plenum, 1969.



Jiang Jin received the B.S. and M.S. degrees in engineering mechanics from the Liaoning Technical University, Fuxin, Liaoning, the People's Republic of China, in 1985 and the China University of Mining and Technology, Xuzhou, Jiangsu, the People's Republic of China, in 1988, respectively; and the Ph.D. degree in measuring technology and instruments from Nanjing University of Aeronautics and Astronautics, Nanjing, Jiangsu, the People's Republic of China, in 1998. Since 1988 he has been with Nantong University (formerly

called Nantong Institute of Technology), where he is currently an associate professor of engineering mechanics.

His research interests include smart material and structures, finite-element method, and solid mechanics.



Romesh C. Batra, the Clifton C. Garvin Professor of Engineering Science and Mechanics at Virginia Polytechnic Institute and State University, Blacksburg, VA, earned his B.Sc. (Mech'l Eng'g) degree from the Thapar College of Engineering (now called Thapar University), Patiala, India, in 1968, the M.A.Sc. (Mech'l Eng'g) degree from the University of Waterloo, Waterloo, Ontario, Canada, in 1969, and the Ph.D. degree in mechanics and materials science from the Johns Hopkins University, Baltimore, MD, in 1972.

His teaching and research activities have earned him the grade of Fellow of the American Society of Mechanical Engineers (ASME), the American Academy of Mechanics, the Society of Engineering Science, and the American Society of Engineering Education, induction into the Hopkins Society of Scholars, the Alexander von Humboldt Award in 1992, and the Reissner Medal from the International Society of Computational Engineering Sciences. He served as President of the Society of Engineering Science in 1996. His research interests include smart materials/structures, ductile failure, penetration mechanics, computational mechanics, and functionally graded materials.